Energy and Buildings 158 (2018) 1711–1723

Contents lists available at ScienceDirect

Energy and Buildings

journal homepage: www.elsevier.com/locate/enbuild

# Empirical and comparative validation of an original model to simulate the thermal behaviour of outdoor test cells

G. Cattarin[a,b,c,*], L. Pagliano[a], F. Causone[a], A. Kindinis[b,c]

[a] end-use Efficiency Research Group, Department of Energy, Politecnico di Milano, Via Lambruschini 4, 20156, Milano, Italy
[b] Université Paris-Est, Institut de Recherche en Constructibilité, ESTP, F-94230, Cachan, France
[c] Efficacity, 14-20 boulevard Newton, 77447 Marne la Vallée Cedex 2, France

ARTICLE INFO

*Article history:*
Received 24 March 2017
Received in revised form 5 November 2017
Accepted 24 November 2017
Available online 26 November 2017

*Keywords:*
Guarded test cell
Experimental validation
Code-to-code comparison
Intermodel comparison
Matlab
Trnsys

ABSTRACT

Calorimetric methods for the performance assessment (e.g. for the determination of the solar factor) of transparent building components have been largely applied in indoor laboratories under steady-state conditions and in outdoor test cells under dynamic boundary conditions provided by real weather. In the latter case the accuracy of the measurements depends significantly on the temporary storage of energy in the test cell envelope. An analysis by Pagliano et al. (2017) developed a dedicated lumped thermal model in Matlab environment in order to improve the design of calorimeters for the measurement of the solar factor by minimizing the energy storage effects in the envelope of the calorimeter and estimating precisely their entity. The developed model was based on literature studies on buildings' dynamic energy simulations and adopted some common hypotheses used by existing building energy simulation software tools. However, when modelling light-mass and highly insulated buildings, such as test cell facilities, small variations in the power inputs can generate significant variations of the internal temperatures, challenging for the model to follow accurately. In order to verify the accuracy of the developed model in predicting the thermal behaviour of an outdoor test cell, an extensive validation work has been carried out. In particular, this paper summarises (i) an experimental validation carried out using a data set from the BESTLab facility, located at the research centre Électricité de France R&D Les Renardières (FR) and (ii) an intermodel comparison between the code developed in the Matlab environment and TRNSYS, a well-established building energy simulation tool.

Concerning the validation at the BESTLab, the results show that the model is able to predict the temperature evolution of the internal air and of the internal surfaces of the envelope with good accuracy, with residuals lying within a range of $\pm 1$ °C; reasons for discrepancies between measurements and predictions are discussed in the paper. As regards the intermodel comparison, the correspondence between the two software tools is generally good, with residuals lying most of the time within a range of $\pm 0.5$ °C. The residuals are lower for the intermodel comparison, partly because input values are in this case not affected by uncertainty. Although TRNSYS and the developed *Matlab code* adopt some similar assumptions and simplifications, they also present some modelling differences that are highlighted in the paper.



## 1. Introduction

Before presenting the verification and validation activities, for sake of clarity we briefly discuss in Section 1.1 the distinction between the terms *verification*, *validation* and *calibration*. Section 1.2 summarises the most common approaches adopted for the validation of building energy software tools, while Section 1.3 presents the goals and limits of the present verification and validation process.

### 1.1. A conceptual distinction: verification, validation and calibration

The terms *verification*, *validation* and *calibration* are sometimes used with relatively vague definitions or even as synonyms, however their meaning is essentially different, as discussed in detail in Trucano et al. Trucano et al. (2006). The authors compare existing definitions of *verification* and *validation* used in the field of computational science and engineering and propose a definition of

* Corresponding author at: end-use Efficiency Research Group, Department of Energy, Politecnico di Milano, Via Lambruschini 4, 20156, Milano, Italy.
*E-mail address:* giulio.cattarin@polimi.it (G. Cattarin).

https://doi.org/10.1016/j.enbuild.2017.11.058
0378-7788/

the *calibration* process and other related terms. In particular, they report the definitions by the US Department of Energy's Advanced Simulation and Computing (ASC) program:

- *verification* is the process of confirming that a computer code correctly implements the algorithms that were intended,
- *validation* is the process of confirming that the predictions of a code adequately represent measured physical phenomena.

Trucano et al. [1] provide the following definition of calibration:

– *calibration* is the process of improving the agreement of a code calculation or set of code calculations with respect to a chosen set of benchmarks through the adjustment of parameters implemented in the code.

The authors define a *benchmark* as «a choice of information that is believed to be accurate or true for use in verification, validation or calibration». Trucano et al. [1] consider that calibration should not be used to increase the credibility of a certain program. The calibration process has «questionable explanatory or predictive content» and it does not answer to the questions posed by the validation process nor it addresses verification: «the question of correctness of solution algorithms, their bug-free software implementation, and the particular mathematical accuracy of numerical solution of equations is not answered by comparison with experimental data, nor by tuning the computed agreement with experimental data» [1]. However, calibration has often been associated to the model validation process. For example, within the framework of the IEA Task 22 (Building Energy Analysis Tools), Palomo del Barrio and Guyon [2] propose model diagnosis and parameter estimation techniques which are intended to fine-tune the model parameters and improve the match between measurements and predictions. Still, in a validation/calibration exercise in various rounds conducted within IEA-Task 22, it was underlined that «Legitimate changes had to have a reasonable physical basis. Changes could not be made just to better match the measured data» [3]. A common strategy is that of calibrating a model on a certain data set and then testing it on a different data set in order to check the model reliability, a phase called *model corroboration* in Mara et al. [4] and Miranville et al. [5].

In the present work, the main objective is to improve the quality of the match (in other terms, to reduce the size of residuals) only by physical considerations; the model parameters are kept at their *nominal values* (e.g. the values provided by the technical sheets of the building materials). Therefore, we follow the view presented by Trucano et al. [1] and we exclude the calibration phase from the present validation process.

The following Section focuses on the validation of building energy software tools, summarising basic concepts and classifications such as *internal vs external* errors, and the distinctions between *empirical, analytical* and *comparative* validation methods.

### 1.2. Validation of building energy software tools

The scientific community generally agrees on considering the validation of a building simulation tool as a complex process, which undergoes a trade-off between the immense number of possible combinations of inputs and the limitations given by computational time and developers' effort ([6,7]). Each software tool relies on a certain number of elementary models that describe specific physical phenomena; these models are expressed by analytical formulae or (semi-)empirical correlations and are based on a set of hypotheses which limit their field of application. Last but not least, the correlations are translated by a (human) software developer into lines of code that can be interpreted and executed by a machine. So-called *internal errors* (using a classification by [8] may occur at any stage of this process, starting from the simplifications that models adopt to describe complex physical phenomena down to the coding and the numerical computation performed by the machine. The results provided by a software tool are also affected by *exter-*

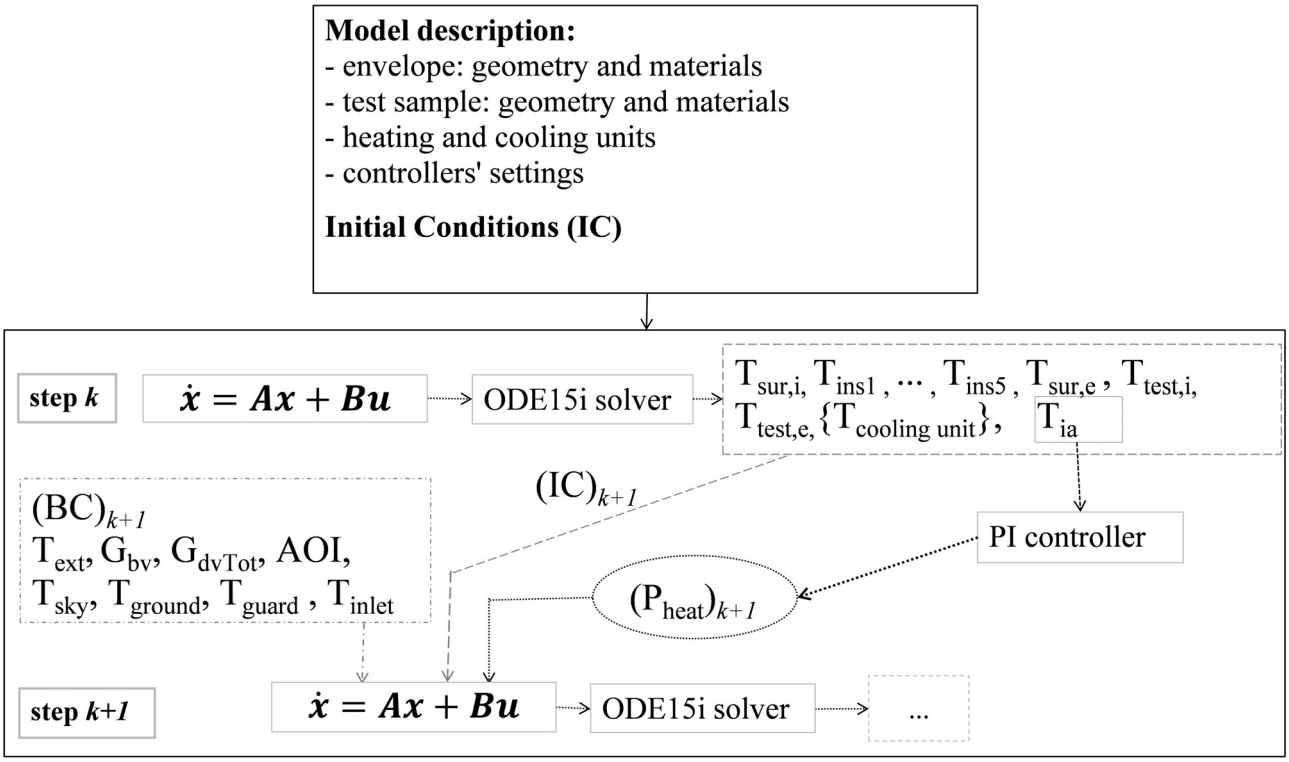


**Fig. 1.** Structure of the Matlab code. The term {Tcooling unit} refers to the temperature nodes in the cooling unit (metallic parts and water layer).

*nal errors*, which are caused by differences between the simulation inputs and the *reality* (i.e. weather conditions, occupant behaviour, geometry of the envelope, materials' properties, building layout, description of heating/cooling systems, etc.).

Validation should hence be seen as an ongoing process, undertaken by both program developers and users, that gradually improves the program reliability by identifying possible internal errors [9]. This requires that external errors are minimized, for example by using a well-known and highly monitored test cell and a high-quality weather data set (in empirical validations, see further on) or by feeding the program under validation and one or more validated programs with the same input data (in comparative validations, see further on). Finally, one should remember that the validation process requires a human intervention, and thus the validation process tests, up to a certain extent, the combination of the user's skills, the software and, in case of an empirical validation, the experiment itself ([6,3]).

In the last decades, various validation techniques have been developed in order to increase confidence in models and simulation codes. The most well-known classification of validation methods, reported by Judkoff et al. [10] and adopted by current standards such as ANSI-ASHRAE 140-2017 [11], highlights three complementary approaches, that is the analytical verification, the comparative testing and the empirical validation. The reader can refer to the works by Judkoff et al. [7] and Xiao [12] for additional information on analytical verification. *Comparative testing* (also called *inter-model, code-to-code or software-to-software comparison*) has often been implemented thanks to its flexibility (being applicable to arbitrarily complex models) and its rapidity of implementation [12]. The occurrence of differences in the results provided by two programs does not necessarily mean that the program under validation is faulty, since the discrepancies could arise from different model hypotheses; in other terms, there is no truth standard [13]. However, «Collective experience in this task has indicated that when programs show major disagreement with a range [*of results given by other software tools*], there is often find [*sic*] a bug, a questionable algorithm, or an input error caused by faulty or ambiguous documentation» [14]. The highest reliability in intermodel comparison can be obtained by simulating a number of different test cases and adopting various modelling and solving approaches [7]. *Empirical validation* has gained great popularity due to its attempt to deal with real-world complexity, since it tests a program under situations similar to those encountered in design studies [15]. In Irving's words, empirical validation «[. . .] is the foundation stone of modern science which has superseded subjective philosophical conjecture» [16]. However, the limits of empirical validation lie in the «need for high levels of instrumentation, consideration of all heat and mass flow paths/processes, accurate control and minimisation of uncertainty» [17]. Due to the cost of experimental set-ups, empirical validation tests have been historically more challenging than comparative and analytical tests [3]. In a recent literature review, Cattarin et al. [18] present an overview of experimental studies that adopted outdoor test cell facilities to validate airflow and daylight models and to characterize the thermal performance of single building components or control systems. The review reports and discusses also potential sources of discrepancy between measurements and numerical predictions.

### 1.3. The present verification and validation process

The RC thermal model of a calorimetric test cell, presented in [19] has been specifically developed for the purpose of designing a more precise and accurate outdoor solar calorimeter. One of the main goals of the study in [19] is to investigate the impact of the variation of the internal energy of the calorimeter on the determination of the solar factor of transparent components. The core part of the code models: • the transparent element and the way it filters the solar radiation, • the envelope dynamics and its interaction with entering radiation, internal air and the surrounding environment, and • the heat extraction process. It can be specialised to various cell configurations and heat extraction strategies and in the cited paper it has been used to model: one traditional test cell where entering radiation is absorbed by the internal surfaces of the cell, transferred by convection to internal air and finally extracted via a cooling coil (TRAD); one where a thin metal screen absorbs the entering radiation before releasing it to the air (SCREEN); and a third where a cooled metal plate intercepts the radiation and extracts it from the cell (SOLAR).

Fig. 1 shows the software structure, developed in Matlab for the purpose of integrating the differential equations of the model. The first block of code creates the materials' library and assigns the features of the heating and cooling systems (e.g. range of operation) and the parameters of the regulation system (e.g. set-point temperature, proportional and integrative coefficients of the controller for the heating unit). A sub-function creates the initial matrices A and B and the vector u of the state-space which express the system of ordinary differential equations. The system is integrated by the ODE15i solver of Matlab, which provides solution values for a time interval of 5 s.

Then the code updates the boundary conditions including the relative position of the sun. The cooling coil power rate is adjusted based on the extra-terrestrial solar radiation in order to get smooth operation, while a fast fine tuning of the *net* power extraction from the test cell is provided by adjusting the power delivered by the electric heater based on the level of internal air temperature. In particular, the electric heating power is updated every 10 s, while the water mass flow rate and, for the cases SCREEN and TRAD, the convective heat transfer coefficient (controlled by the fan's

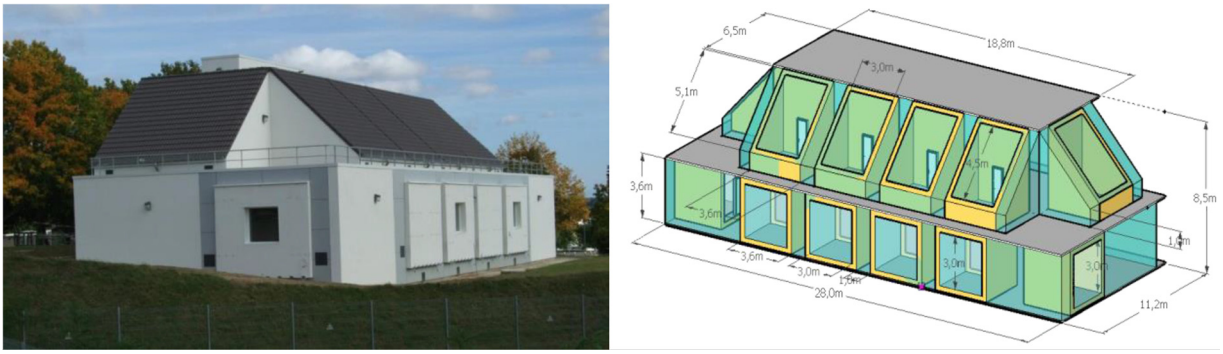


**Fig. 2.** BESTLab Platform: external view (with indication of the test cell used in the present work) and scheme. Sources: Bontemps et al. Bontemps et al. (2015) and EDF (2016).

**Table 1**
Stratigraphy of the walls facing the guard zone.

| Walls facing guard zone | thickness (m) | thermal conductivity ($W m^{-1} K^{-1}$) | density ($kg m^{-3}$) | specific heat ($J kg^{-1} K^{-1}$) |
|---|---|---|---|---|
| two fibre-gypsum panels | 0.026 | 0.32 | 1150 | 1265 |
| mineral wool | 0.045 | 0.04 | 39 | 1400 |
| two fibre-gypsum panels | 0.026 | 0.32 | 1150 | 1265 |
| XPS | 0.200 | 0.029 | 33 | 1400 |
| EPS | 0.100 | 0.032 | 14 | 1400 |
| internal plaster | 0.013 | 0.313 | 816 | 800 |

Source: EDF (2016).

**Table 2**
Stratigraphy of the West wall facing the exterior.

| West wall | thickness (m) | thermal conductivity ($W m^{-1} K^{-1}$) | density ($kg m^{-3}$) | specific heat ($J kg^{-1} K^{-1}$) |
|---|---|---|---|---|
| external coating | 0.010 | 0.5 | 1300 | 1000 |
| hollow cinderblock | 0.200 | 0.8 | 800 | 1000 |
| EPS | 0.100 | 0.032 | 14 | 1400 |
| internal plaster | 0.013 | 0.313 | 816 | 800 |

Source: EDF (2016).

**Table 3**
Stratigraphy of the ceiling slab of the test cell.

| Ceiling slab | thickness (m) | thermal conductivity ($W m^{-1} K^{-1}$) | density ($kg m^{-3}$) | specific heat ($J kg^{-1} K^{-1}$) |
|---|---|---|---|---|
| external gravel | 0.080 | 0.96 | 1800 | 1000 |
| XPS | 0.100 | 0.029 | 33 | 1400 |
| concrete slope | 0.05 | 1.13 | 2000 | 1000 |
| concrete slab | 0.23 | 1.75 | 2500 | 1000 |
| XPS | 0.200 | 0.029 | 33 | 1400 |
| EPS | 0.100 | 0.032 | 14 | 1400 |
| internal plaster | 0.013 | 0.313 | 816 | 800 |

Source: EDF (2016).

**Table 4**
Stratigraphy of the floor slab in contact with the unconditioned technical space.

| Floor slab | thickness (m) | thermal conductivity ($W m^{-1} K^{-1}$) | density ($kg m^{-3}$) | specific heat ($J kg^{-1} K^{-1}$) |
|---|---|---|---|---|
| external plaster | 0.013 | 0.313 | 816 | 800 |
| three XPS panels | 0.300 | 0.029 | 33 | 1400 |
| concrete slab | 0.23 | 1.75 | 2500 | 1000 |
| XPS | 0.100 | 0.029 | 33 | 1400 |
| internal wood panel | 0.022 | 0.12 | 1250 | 1200 |

Source: EDF (2016).

**Table 5**
Thermo-optical properties of the glazing system at normal incidence and thermal transmittance of the window.

| Global optical properties | | | Single pane | Thermal properties |
|---|---|---|---|---|
| solar direct transmittancep at normal incidence ($\tau_{12}$) | solar direct absorptance ($\alpha_{Tot}$) | solar direct reflectance ($\rho_{12}$) | solar direct absorptance ($\alpha_1$; $\alpha_2$) | window thermal transmittance $U_w$ ($W m^{-2} K^{-1}$) |
| 0.52 | 0.19 | 0.28 | 0.099; 0.095 | 1.12 |

Source: EDF (2016).

speed) are updated every 60 s. The radiative heat transfer coefficients are recalculated based on the surface temperatures. The angular-dependent thermo-optical properties of the window are re-calculated based on the updated relative position of the sun.

The developed Matlab code is based on literature studies on buildings energy modelling and adopt hypotheses used by validated building energy simulation tools. However, when modelling light-mass and highly insulated buildings, such as test cell facilities, small variations in the power inputs can generate significant variations of the internal temperatures, challenging for the model to follow accurately. For this reason, great care should be taken to correctly describe the interaction of this type of constructions with the external environment, in particular concerning the rapidly variable stimulus of solar radiation. We have hence used the Matlab code to model a specific test cell for which a reliable dataset is available and the physical configuration of the cells and sensors is known, thanks to the collaboration with the laboratory of EdF at the site of Les Renardières, France.

The order of the model has been chosen based on literature and the need for accuracy in the evaluation of the energy flows at the surfaces and of the penetration of the thermal wave (Section 2.2).

The first experimental validation compares our code developed in the Matlab environment (*Matlab code* from hereon) to the *benchmark* (as defined in Section 1.1) represented by a data set measured in July 2014 at the BESTLab facility located at the research centre Électricité de France R&D Les Renardières. As it is usually the case of test cell experiments, the facility was kept closed during the whole experimental campaign and no direct human interaction was allowed for. Therefore, the simulation activity excludes any occupant effect and can be classified as an *idealized study* according

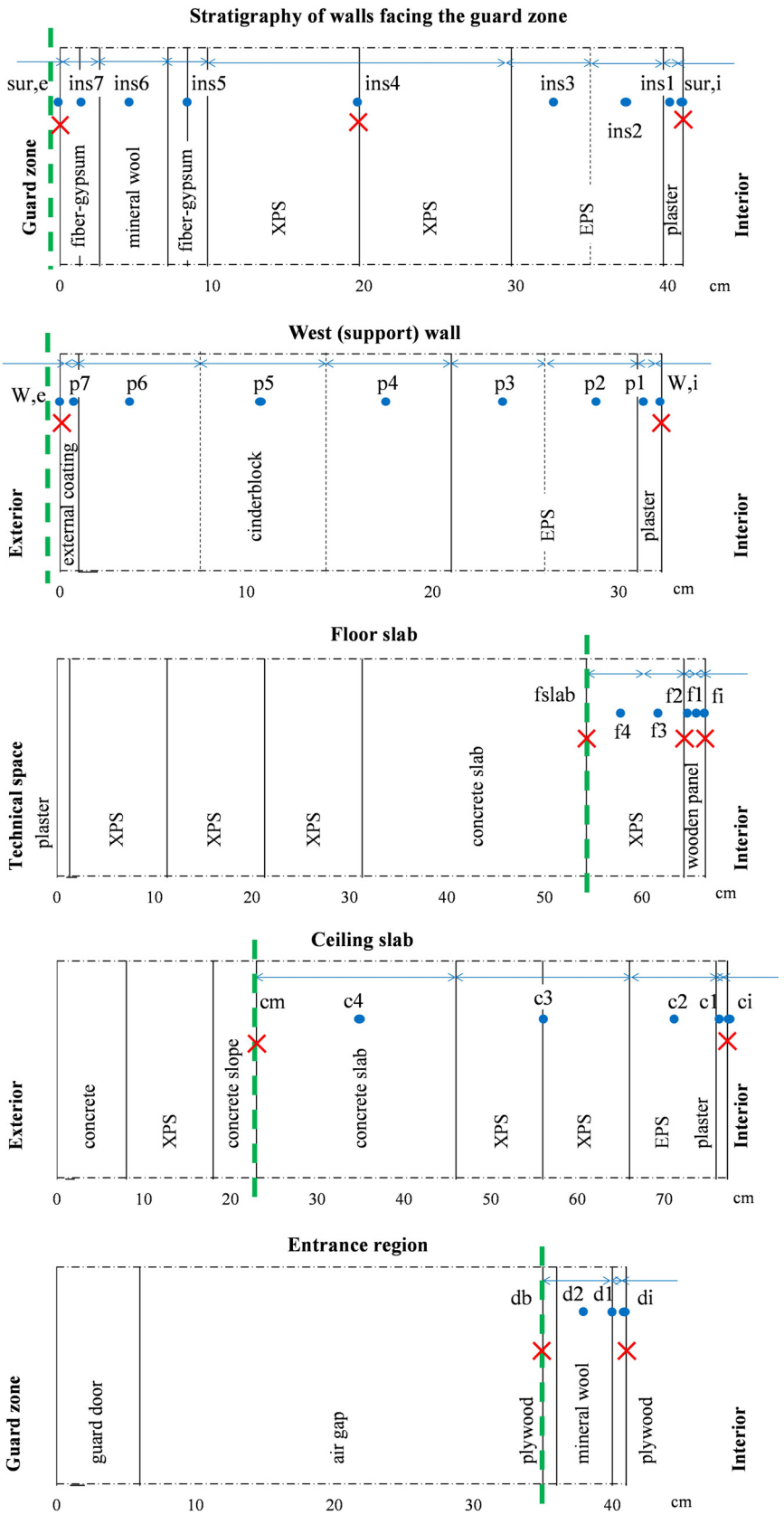


**Fig. 3.** Thermal nodes assigned to the test cell's envelope. The red crosses represent the physical location of the sensors, while the blue circles correspond to the thermal nodes of the model. The blue arrows indicate the layer/layer's slab represented by a certain node. The green dashed lines indicate the boundaries of the control volume described by the thermal model. (For interpretation of the references to colour in this figure legend, the reader is referred to the web version of this article.)

to Ryan and Sanquist [20]. The experimental validation is reported in Section 2. Section 5 reports the main results of an *intermodel comparison* between the *Matlab code* and TRNSYS, which is a widely used building energy software tool (BEST directory [21]). Within the intermodel comparison we first checked individual algorithms, such as those used for the astronomical calculations (this phase can be intended as a *model verification*, since the two codes use the same algorithms), and then we compared the global thermal behaviour of a virtual test cell, modelled using respectively our Matlab code and TRNSYS.

Judkoff et al. [7] point out that «The comparative technique may be used before empirical validation studies (...) to identify the need for empirical validation and to define the level of empirical validation needed». In the present case, the thermal model tested within the intermodel comparison is very similar to the one used in the empirical validation at the BESTLab facility. The two validation activities have actually been run in parallel, and should be considered concurrent rather than sequential.

The general goal of this validation activity is to check whether the code developed for the thermal simulations presented in [19] provides accurate predictions of internal temperature levels. The core part of the code models: • the transparent element and the way it filters the solar radiation, • the envelope dynamics and its interaction with entering radiation, internal air and the surrounding environment, • the heat extraction process. The hypotheses and algorithms of this core part are the object of the present validation work and are presented in Section 2.2. We have to this purpose used in this paper the core Matlab code to model the specific configuration of the BESTlab and compare its predictions with the available experimental benchmark provided by the BESTLab facility.

A separate publication will present a second experimental validation at the ZEB Test Cells laboratory (Trondheim, NO). This second validation is accompanied by a sensitivity analysis highlighting the parameters and inputs that are most influential on the thermal behaviour of the test cell under study. The study includes an in-depth introduction on the specific features of lumped-parameter thermal models for building energy simulations.

## 2. Experimental validation at the BESTLab facility

### 2.1. Description of the facility

The BESTLab (Building Envelope and Solar Technologies Laboratory) facility, represented in Fig. 2, was built in 2010 at the site of EDF R&D Les Renardières, which is situated about 75 km south of Paris. The facility is surrounded by a lawn for a distance of at least 200 m on the east, south and west sides.

The facility hosts twelve independent cells distributed on two floors; the cells at the ground floor are conceived to test vertical façade components, while sloped roof components can be installed on the upper cells. The facility can be classified as *comparative and guarded* [18], since it is possible to simultaneously expose two or more technologies on the South façade (comparative approach) but also to obtain performance assessments in absolute terms by means of a calorimetric measurement in each cell, surrounded (though not completely) by a guard zone.

The test cell used in the present validation is the ground-floor, west-facing cell, indicated by the red box in Fig. 2. The exact azimuth of the external surface is 87° from south, while the geographical coordinates of the cell are: latitude 48°22′ N, longitude 2°49′ E, altitude: 100 m.

#### 2.1.1. Opaque envelope components

The test cell has internal dimensions (WxDxH): 2.89 m × 2.97 m × 2.82 m, with three walls facing the guard zone, the West wall facing the exterior and hosting the test sample, the ceiling slab exposed to external environment and the floor slab separated by the soil by an unconditioned technical space. The layers constituting the envelope elements of the test cell are described in Tables 1–4. All the elements of the building envelope are highly insulated (thermal transmittance $U < 0.1\ W\,m^{-2}\,K^{-1}$), while the entrance region is constituted by two sealed doors separated by a buffer zone (internal door: sandwich panel with 4-cm mineral wool layer between two plywood panels). The absorptance and the surface emissivity of the plaster on the internal surfaces of the walls were experimentally determined to be 0.77 and 0.94, respectively [22].

The airtightness level, ensured by a film of polyethylene and silicone joints, was checked in April 2013 (while the measurement period considered is July 2014) by means of a depressurization system and the infiltration air flow rate under 4 Pa pressure difference resulted $Q_{4Pa,ATBat} = 0.04\ m^3\,h^{-1}\,m^{-2}$ (calculated according to the standard [23]), which confirms the quality of the sealing at the critical points in the test cell.

#### 2.1.2. Transparent component

The window installed on the West wall is composed by an argon-filled (90%) double glazing of total dimensions 1400 mm × 1440 mm (dimensions of the glazed part 1317 mm × 1317 mm), with a low-emissivity coating and a PVC frame. Its thermo-optical properties according to the manufacturer are reported in Table 5. The angular-dependent properties were calculated using the WINDOW tool v7.4.8.0 [37] as described in the modelling hypotheses (Section 2.2).

#### 2.1.3. Measurement set-up

The test cell is fully instrumented in order to monitor the temperatures of the envelope and of the internal air (using 4-wires, 1/3 DIN platinum resistance thermometers with accuracy ± 0.2 °C) and to keep track of the energy inputs due to the mixing fan. Reference [25] describes in detail the positions of the temperature sensors on each surface and within the walls. The internal-air temperature sensors are shielded against solar radiation and installed at three heights (0.5 m, 1.5 m and 2.5 m) in order to check possible air temperature stratifications. In addition, the globe temperature is measured by resistance thermometers inserted into black globes of 15 cm and 9 cm of diameter, both at 1.5 m height. The air temperature in the guard zone is measured by shielded resistance thermometers placed at about 20 cm from each wall of the test cell. The ceiling slab is monitored by one sensor placed on its internal surface and two sensors positioned above the concrete slab. The entrance region is monitored by sensors placed on both sides of the two doors separating the guard zone from the test cell. Concerning the floor slab, eleven sensors are installed between the insulation layer and the concrete slab. While thermal bridges have been drastically reduced in 2013 after a dedicated study (mentioned in [26], critical points are still present at the interfaces between the (removable) West wall and the (fixed) envelope. Therefore, the sensors in the floor slab monitor the temperature distribution and may be used to estimate the impact of the remaining thermal bridges. The temperature of the exterior surface of the West wall is measured at four different locations to check its temperature uniformity.

The data set used for the present validation was recorded in July 2014, when the heater was off (test cell in free-floating mode) while the mixing fan was running at constant speed (measured electrical power consumption approximately constant at 5 W). The external weather conditions are measured at a weather station close to the BESTLab; its characteristics are reported in Table 6. Two pyranometers and a pyrheliometer, mounted on a sun tracker, measure separately the global and diffuse solar irradiance on the horizontal plane and the beam normal irradiance. The external air tempera-

**Table 6**
Characteristics of the sensors installed at the weather station next to the BESTLab facility.

| physical variable | type of sensor | accuracy |
|---|---|---|
| External air temperature | Pt100 1/3 DIN RTD | ±0.2 °C |
| Sky temperature | pyrgeometer | ±2 °C |
| Relative humidity | optoelectronic | ±1% |
| Wind speed, wind direction (3 m height) | helix | ±0.3 $ms^{-1}$,±10% |
| Global irradiance (tracker) | pyranometer | ±1.5% |
| Diffuse irradiance (tracker) | pyranometer | ±1.5% |
| Beam normal irradiance (tracker) | pyrheliometer | ±1.5% |

ture is measured at a height of 2.5 m by a shielded and mechanically ventilated thermo-resistance. Additional weather data are collected on the West façade. In particular, a pyranometer is installed on the façade to measure the global solar irradiance on the vertical plane of the test sample (accuracy ± 2%). The present validation is conducted over the period 3rd – 30th July 2014 (28 days); as already mentioned, during this period the test cell was in free-floating mode. Free-floating periods and clear sky conditions are of particular interest in the validation process, since the test cell experiences large temperature swings due to the entering solar load (and secondarily due to external temperature variations) and thus the model is challenged in its ability to predict the temperature variations.

### 2.2. Thermal modelling of the BESTLab test cell

We summarise here the hypothesis implemented in the matlab code in order to achieve a model corresponding to the main physical configuration and sensor setup of the BESTLab. Thanks to the good air temperature uniformity in the room achieved by the mixing fan, the internal air can be assumed at approximately uniform temperature and represented by a single thermal node; air infiltration can be neglected due to the high airtightness level. The mechanical power used by the mixing fan is assigned as internal energy to the node representing the internal air. The overall thermal capacity of the lamp, the heater, the mixing fan and the metallic masts that hold the temperature sensors has been estimated at 50 $kJ\,K^{-1}$ (equivalent to 100 kg of steel) and assigned to the internal air node.

The North, East and South walls have the same stratigraphy and are in contact with the guard zone, where the air temperature can be considered uniform with good approximation. Previous studies have used a limited number of capacitive nodes (between one and four) to simulate the heat flows through envelope components (e.g. [27] and [28]). However, given the complex stratigraphy of the envelope of the test cell under analysis, we performed some preliminary simulations representing at least each stratum with a node and then we gradually increased the number of capacitive nodes by adding more nodes close to the surfaces. We added nodes until the differences in the computed surface temperatures (which are connected to the convective and radiative exchanges) between the model of order *k* and the model of order *k-1* became negligible (±0.05 °C) for the expected fluctuations of the boundary conditions. Therefore, these three walls are here represented by a ninth-order element (11R9C). The West wall and the entrance door are represented by a ninth-order element (11R9C) and a fourth-order element (6R4C), respectively. The boundary condition of the entrance door is the temperature of the node *db* in Fig. 3. The floor slab is in contact with a free-floating technical space. Since the technical space is not monitored, the chosen boundary of the thermal model is the bottom surface of the XPS layer, which is monitored by eleven sensors (Section 2.1.3).

A simple average of the values registered by the eleven sensors would not take into account the fact that the sensors in the centre of the room are representative of a larger surface area, while others are installed in correspondence of peripheral zones affected by thermal bridges and hence monitor more local phenomena. We decided to assign to each sensor a specified surface area that can be considered, as a first approximation, at uniform temperature, as described in [25]. The ceiling slab is in contact with the exterior. We excluded the top-gravel layer and the top-concrete layer from the control volume, since these layers retain rainwater and their thermal conductivity are expected to vary significantly with the water content. Therefore, only the bottom part of the concrete ceiling slab is included in the model and the boundary condition is provided by the two sensors placed above the slab (node *cm* in Fig. 3).

Fig. 3 shows the thermal nodes in each component of the envelope as blue circles, while the blue arrows indicate the layer, or the portion of a certain layer, assigned to each thermal node. The red crosses represent the physical location of the sensors. The green dashed lines indicate the boundaries of the control volume described by the thermal model.

The internal layer of plaster of the walls, the internal plywood panel of the door, the wooden flooring and the external coating of the West wall are described by two-to-three nodes in order to better predict the thermal dynamics resulting from rapid fluctuations of solar radiation (e.g. due to transient clouds). The nodes in the central layers of the envelope are more spaced since they are involved in slower dynamics, such as daily cycles. Similar considerations are used extensively in finite-element studies, where the solid mesh is refined close to the surfaces (e.g. [26]. The simulation is conducted using the nominal values of the materials' thermal properties and neglecting thermal bridges (hypothesis of mono-dimensional heat flows).

The nodes corresponding to monitored points are assigned initial conditions equal to the measured values, while the additional nodes (blue dots in Fig. 3) are assigned initial conditions assuming, as a first approximation, a linear temperature profile across each layer of the envelope.

Concerning the convective heat exchanges, we adopt the correlations (valid for temperature differences between surface and air <5 °C) proposed by Khalifa and Marshall [29] for vertical walls, floor and ceiling surfaces. The simulation results show that, due to the small air-surface temperature differences measured at the BESTLab (consequence of the high level of insulation and airtightness and the operation of the mixing fan), these correlations provide values generally below 1.5 $Wm^{-2}\,K^{-1}$. Similar values are obtained using the correlation proposed by Hatton and Awbi [30] for vertical surfaces. Regarding the long-wave heat exchanges, we adopt the so-called *zonal method* described by Rohsenow et al. [31].

The entering solar radiation is composed by a beam component and a diffuse component. Being non-directional, the *diffuse component* is usually attributed to the internal surfaces in simple ways, without accounting for the sun position. For example, the commercial software TRNSYS distributes the diffuse radiation according to the absorptance-weighted area ratios of each surface. The beam component has been treated in various ways in the literature. Chatziangelidis and Bouris [32], Kontoleon [33] and ASHRAE Fundamentals (2009) [34] offer details on the subject. In the present work, we take into account the different absorptances of the walls and the floor, and the fact that a fraction of the entering solar radiation re-escapes through the window. More details are reported in [25].

The window is modelled by two thermal nodes, one for each glass pane. The thermo-optical behaviour of the transparent test sample is described considering the dependency of the glazing properties on the angle of incidence of beam solar radiation, while the behaviour of the test sample under diffuse radiation is treated, as suggested by Duffie and Beckman [35] and Davies [36], considering an *equivalent angle of incidence* of 60°. Since the angular-dependent optical properties of the window were missing

**Table 7**
Performance indicators (period 3rd – 30th July): root mean square error (RMSE), mean residuals ($\varepsilon_{mean}$) and standard deviations of residuals (SD ($\varepsilon$)).

| | Air,int | Surf,int | West,int | Floor,int | Ceiling,int | Door,int |
|---|---|---|---|---|---|---|
| RMSE (°C) | 0.54 | 0.45 | 0.11 | 1.13 | 1.03 | 0.65 |
| $\varepsilon_{mean}$ (°C) | 0.07 | −0.02 | −0.06 | −0.50 | −0.85 | −0.45 |
| SD($\varepsilon$) (°C) | 0.54 | 0.45 | 0.10 | 1.01 | 0.57 | 0.47 |

in the technical sheets provided by the manufacturer, we calculated them using the software tool WINDOW v7.4.8.0 by Berkely Lab [37], choosing from the software library the glass panes that are most similar to the ones installed in the window (an external pane Saint Gobain Planiclear and an internal pane Planitherm One, with a low-emissivity coating on face 3). The calculated solar direct transmittance at normal incidence ($\tau_{12,calculated} = 0.43$) differs significantly from the one declared by the manufacturer ($\tau_{12,declared} = 0.52$, Section 2.1.2); we decided to adopt the values calculated with WINDOW since no testing/calculation methodology was reported in the technical sheets. The frame has not been modelled separately; the correspondent front area has been treated as if it were occupied by the support wall. The window is installed on a support wall; the external glass pane is at a 30 cm distance from the external surface of the support wall. The support wall partially shades the window from beam solar radiation, and the effective surface area $A_{eff,glz\_beam}$ of the window that is hit by beam solar radiation (also expressed as *sunlit fraction of the total window area* in [38] is a function of the geometry of the window and of the relative position of the sun. Further details on the determination of $A_{eff,glz\_beam}$ is reported in [25]. In order to correctly model the behaviour of the window when exposed to diffuse and beam radiation, it is necessary to split the global irradiance values measured by the pyranometer on the West façade into a beam and a diffuse component. The beam component BeamWest on the West façade is calculated from the beam normal radiation measured by the pyrheliometer and the angle of incidence of beam radiation on the west-exposed façade. The total diffuse component (sum of the sky-diffused and the ground-reflected radiation) is simply derived as difference between GlobalWest and the beam component BeamWest. Additional considerations on the external boundary conditions (external air temperature, sky-dome temperature, ground-surface temperature, external wind speed) are reported in [25].

## 3. Results

As mentioned before, the present simulations are conducted over the period 3rd – 30th July 2014 (28 days). Measurement uncertainty bands are not plotted since the measurement uncertainty for air and surface temperatures (± 0.2 °C) is too small to be visible in the graph. The temperature profiles of the North, East and South walls are represented in Fig. 4 (top), while the temperatures of the floor and ceiling are reported in Fig. 4 (middle). It can be observed that in general there are some discrepancies and their potential causes (e.g. thermal bridges not treated by the model) are discussed in Section 4. For example, the dependence of thermal conductivity of envelope elements on water content is not modelled; this might produce significant effects on the heat flows through the ceiling slab and the West wall, which are exposed to precipitations.

The residuals of the simulation (calculated as *measured minus predicted*) for the internal air and the internal surface temperatures are reported in Fig. 5. The residuals lie most of the time within a ± 1 °C interval. It is possible to notice a daily variation of the residuals, corresponding to the peaks of solar irradiance.

Table 7 reports the performance indicators of the simulation run. The highest values of the Root Mean Square Error (RMSE) are relative to the floor and the ceiling surfaces. The mean value and the standard deviation of the residuals relative to the internal air temperature are comparable with the results obtained by Palomo del Barrio and Guyon [2] for the *nominal model* (model with nominal values of input parameters, i.e. before running a parameter optimization), during an empirical validation conducted at the ETNA facility ($\varepsilon_{mean} = -0.22$ °C, SD($\varepsilon$) = 0.72 °C).

## 4. Discussion

The developed model is generally able to predict the thermal behaviour of the test cell in terms of the evolution in free floating of the temperatures of the internal air and the internal surfaces using as input the measured outdoor conditions. However, residuals show a systematic correlation with the profiles of solar irradiance and external air temperatures. Potential reasons for these discrepancies are discussed below.

### 4.1. Thermo-optical properties of the window

One of the main challenges of the validation process came from the scarce information provided by the manufacturer regarding the thermo-optical characteristics of the window installed on the West wall. In particular, no information was available concerning the angular-dependency of the direct solar transmittance $\tau$ of the specific commercial glass panes constituting the double-glazing unit; therefore the angular-dependent optical properties were calculated using WINDOW tool and choosing from the software library the glass panes that are most similar to the ones installed in the window. The $\tau$ value at normal incidence provided by the manufacturer was higher than the one calculated using the WINDOW tool. We decided to adopt the values calculated with WINDOW since no testing/calculation methodology was present in the technical sheets provided by the manufacturer.

Additional sources of discrepancy between the calculated and the actual optical properties of the window can arise from deposits of dust or dirt on the glazing surface. In addition, both the nominal values provided by the manufacturer and the angular-dependent values calculated by software tools are determined without considering the variability of the spectral characteristics of solar radiation during the day, or their seasonality. The standard proposed by the National Fenestration Rating Council for the measurement of the Solar Heat Gain Coefficient in outdoor solar calorimeters [39] points out the variability of the SHGC with the solar irradiance conditions. In particular, it reports that «The spectral distribution of both the beam and diffuse solar irradiation at the earth's surface can vary with location, season and time of day. Although these variations are typically not significant when testing the SHGC of clear or lightly tinted and uncoated glazing systems, they can influence the measured results if the test specimen has complex spectral or angular optical characteristics. [...] Also, the SHGC results from the same laboratory on the same test specimen may vary based on the time of year, solar altitude angle and/or time of day it was tested. The magnitudes of the errors that can be introduced from these variations are not large but can be significant, depending upon the degree of spectral and/or angular selectivity inherent in the optical properties of the test specimens used».

In the present study, the transparent component is treated with a low-emissivity coating and it is exposed to solar radiation in the afternoon hours. This could result in an optical behaviour that differs both from calculations and from standardized results obtained in indoor laboratories using a solar simulator.

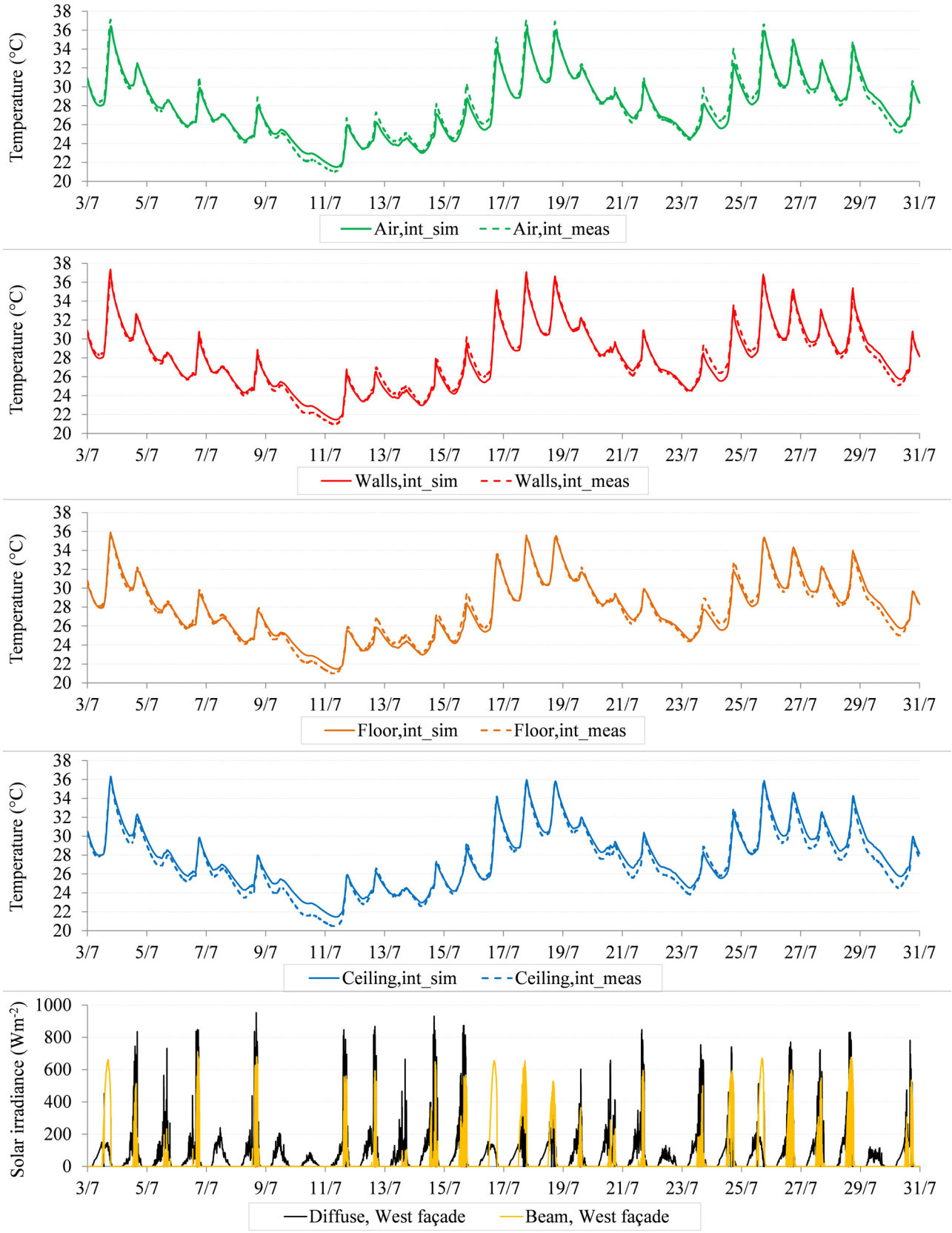


**Fig. 4.** Top four graphs: simulated (sim) and measured (meas) average temperatures of the internal air, the (North, East and South) walls' internal surfaces, the floor and the ceiling. Bottom: diffuse (sky-diffused + ground-reflected) and beam solar radiation on the West façade.

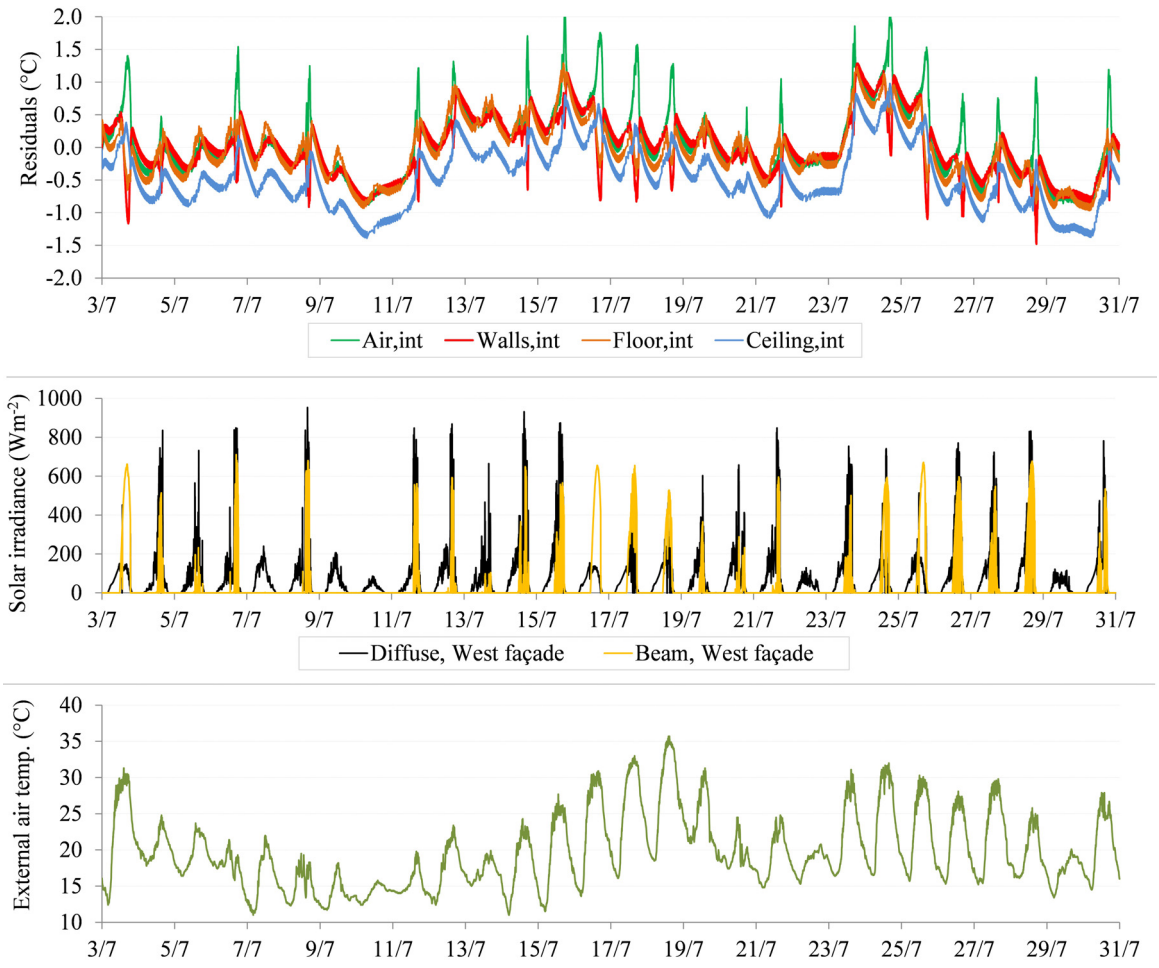


**Fig. 5.** Top: profiles of residuals (calculated as measured minus predicted); centre: total diffuse (including sky-diffused and ground-reflected radiation) and beam solar radiation on a vertical surface exposed to west; bottom: external air temperature.

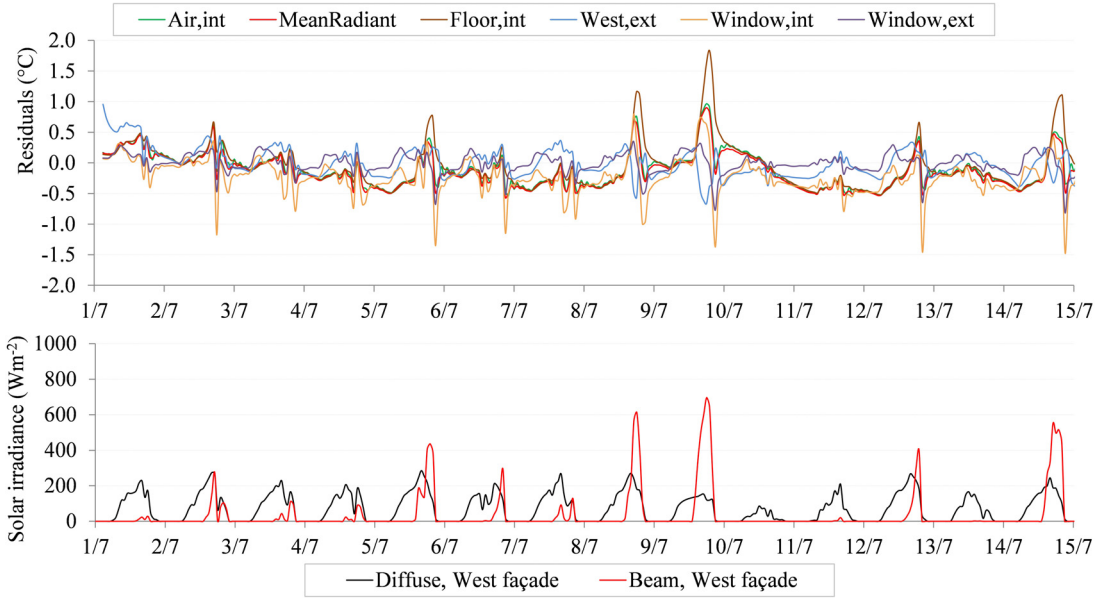


**Fig. 6.** Top: temperature residuals of the intermodel comparison: internal air temperature, mean radiant temperature, floor surface temperature, temperature of the external surface of the West wall, temperatures of the internal and external panes of the window component. Bottom: total diffuse (including sky-diffuse and ground-reflected radiation) and beam solar radiation on a vertical surface exposed to west.

### 4.2. Thermal properties of the envelope and thermal bridges

As highlighted by Judkoff et al. [7], in validation studies it is important to accurately know the thermal properties of the envelope components, which can be determined by destructive and/or non-destructive testing procedures. The present simulation was conducted using the nominal values of the materials' thermal properties and neglecting thermal bridges (hypothesis of monodimensional heat flows). Considering that for most of the time the internal air and the internal surfaces of the test cell are warmer than the external environment and the guard zone, neglecting thermal bridges may have led to an underestimation of the heat losses (and hence contributed to an overestimation of internal temperatures). In addition, the presented model does not treat hygrothermal phenomena, and therefore does not take into account the variation of the thermal conductivity with the water content, which can be significant for hygroscopic materials not protected by a moisture barrier.

### 4.3. Astronomical calculations

An additional source of discrepancy between measurements and predictions might result from errors in the calculation of the sun position and the effective glazing area hit by beam solar radiation. However, an intermodel comparison between the *Matlab code* and TRNSYS, a validated building energy simulation tool, indicates that the astronomical calculations are performed correctly (Section 5.1).

### 4.4. Initial temperatures

An uncertain knowledge of the initial temperature distribution within the envelope may increase the residuals in the first days of the simulation, as shown by Bontemps [40] by means of a local sensitivity analysis. However, the effect of uncertainties on the initial temperature profile in the envelope drops down after a period of a few days, as suggested (i) by the study by Bontemps [40] on the BESTLab facility and (ii) by a sensitivity analysis that we carried out within a second experimental validation at the ZEB Test Cells laboratory (Trondheim, NO), which will be presented in a separate publication.

### 4.5. Temperature uniformity and air temperature stratification

A final remark is that the goal behind the development of the *Matlab code* is to describe the overall thermal behaviour of the test cell, in terms of average temperature of the internal air and the internal and external surfaces of the envelope. Like most building energy simulation tools, the developed *Matlab code* does not handle the non-uniform distribution of the entering beam solar radiation on the internal surfaces, and in particular the position of the solar patch. A more detailed treatment of the solar patch, which requires a longer computation time and more burdensome data analysis, could be justified in case of (i) active envelope elements of the test cell (e.g. cooled ceilings or heated floors), (ii) when investigating local thermal/visual comfort indoor conditions or (iii) when differences in the stratigraphy and boundary conditions of each element may introduce significant errors when handled "globally", that is adopting a single thermal node for each layer of the envelope. An example of building modelling that takes into account the position of the solar patch on the internal surfaces is the work conducted by Rodler [26]. Finally, the *Matlab model* assumed that the internal air is perfectly mixed, thus neglecting air temperature stratification; measurement results show however a limited stratification (within $\pm$ 0.5 °C).

## 5. Intermodel comparison with TRNSYS

As underlined by Jensen (1995) [15], «A comprehensive validation methodology should consist of a literature review, code checking, analytical verification, intermodel comparison, sensitivity studies and empirical validation». As concerns empirical validation, Jensen points out that it should never be used alone, due to the measurement uncertainties and the great complexity of experiments. Therefore, it is always a good practice to perform an intermodel comparison, that is, to compare the developed model to existing, validated software tools. The present Section reports a summary of the intermodel comparison activities which have been conducted using the validated building energy simulation tool TRNSYS v.16.

### 5.1. Comparison of astronomical data

The first part of the intermodel comparison process aims at verifying whether the *Matlab code* can correctly calculate the following astronomical variables:

- solar altitude (or its complementary angle, the solar zenith) and solar azimuth
- angle of incidence of beam solar radiation on a tilted surface with given orientation
- extra-terrestrial solar radiation
- beam solar radiation on a tilted surface with given orientation

As concerns the sky-dome temperature, both TRNSYS and the *Matlab code* adopt the model proposed by Martin & Berdahl [41] based on the dry-bulb air temperature, the sky coverage factor and the emittance of the clear sky. We checked the various steps of the algorithms, i.e. the calculation of the dew-point temperature, the cloudiness factor and the sky temperature. This phase can be considered a *model verification* (Section 1.1), since the two codes use the same algorithms. Since no significant differences were observed between the outputs of the TRNSYS and the *Matlab code* in this area, we moved to the following phase, which is comparing the global thermal behaviour of a virtual test cell as predicted by the two codes.

### 5.2. Comparison of the global thermal behaviour of a virtual test cell

The second and main part of the intermodel comparison focused on the modelling of the opaque and transparent envelope components of a virtual test cell in TRNSYS and in our *Matlab code*. This Section first presents the model (where different from the one used in the empirical validation, Section 2.2), then the boundary conditions, and finally the results and a discussion.

#### 5.2.1. Thermal modelling

The virtual test cell modelled in TRNSYS (using Type 56) is equivalent to the test cell at the BESTLab facility as concerns the stratigraphy of the opaque components (walls, floor slab, ceiling slab and entrance door). The transparent component, chosen among the available windows of TRNSYS library, is a double-glazed, air-filled window (InsulatingGlass, 2.8, Window ID: 1002), of dimensions 1.317 m $\times$ 1.317 m, without frame. The optical properties provided by TRNSYS database derive from calculations by the software tool WINDOW 4.1 [24] and are provided for angles of incidence between 0° and 90° (at steps of 10°) and as hemispherical values. In both models no shading effects due to the external wall are considered (in other terms, the external surface of the window lies on the same plane of the external surface of the wall) and the view factor to the sky dome is 0.5 (unobstructed view).

**Table 8**
Performance indicators (period 1st – 15th July): root mean square error (RMSE), mean residuals ($\varepsilon_{mean}$) and standard deviations of residuals (SD ($\varepsilon$)).

| | Air,int | MeanRadiant | Floor,int | West,ext | Window,int | Window,ext |
|---|---|---|---|---|---|---|
| RMSE (°C) | 0.30 | 0.31 | 0.36 | 0.24 | 0.37 | 0.17 |
| $\varepsilon_{mean}$ (°C) | −0.11 | −0.14 | −0.06 | 0.00 | −0.23 | −0.01 |
| SD($\varepsilon$) (°C) | 0.28 | 0.27 | 0.35 | 0.24 | 0.29 | 0.17 |

The convective heat transfer coefficients in the two codes are set to fixed and identical values ($h_i = 11$ kJ hr$^{-1}$K$^{-1}$ ≈ 3.06 Wm$^{-2}$K$^{-1}$, $h_e = 64$ kJ hr$^{-1}$K$^{-1}$ ≈ 17.78 Wm$^{-2}$K$^{-1}$), thus neglecting the variation of the convective heat exchanges with the temperature difference between the surface and the air and the dependency of $h_i$ on the internal air velocity and of $h_e$ on the external wind speed. The long-wave radiative heat exchanges with the sky dome and the ground surface are treated in TRNSYS by means of a *fictive sky temperature* (combination of the sky-dome and the ground-surface temperatures, weighted according to the relative view factors), while in the *Matlab code* they are treated separately, assuming (as in TRNSYS) that the ground-surface temperature is equal to the external dry-bulb temperature.

The modelled test cell is exposed to the climate weather conditions provided by the Typical Meteorological Year (TMY2) of Paris Montsouris. The temperatures of the guard zone, the floor slab and the ceiling slab (boundaries of the model) are fixed at 20 °C. The internal initial relative humidity is fixed at 30% in order to exclude possible condensation effects, while the initial temperature is fixed at 26 °C. The test cell is assumed perfectly airtight and sealed, hence excluding air infiltration and air renovation; internal gains are set to zero and the test cell operates in free-floating mode. Again, these simplifying hypotheses allow us to focus the attention on the dynamic behaviour of the envelope, limiting other potential sources of discrepancy between the two software tools.

#### 5.2.2. Results and discussion

Fig. 6 shows the residuals of the intermodel comparison, calculated as *TRNSYS minus Matlab*. Peak residuals up to about 1.8 °C can be observed for the floor surface. Compared to TRNSYS, the *Matlab code* underpredicts the temperature of the internal pane of the window, with differences up to 1.5 °C in days with mainly beam solar radiation. The residuals are significantly lower for the intermodel comparison (Fig. 6 and Table 8) than for the experimental validation (Fig. 5 and Table 7), partly because input values are, in the intermodel comparison, not affected by uncertainty, in other words, there are no *external errors*.

## 6. Conclusions

The paper presents the methodology and the main results of two validation activities:

- an experimental validation carried out using an existing data set from the BESTLab facility at the research centre Électricité de France R&D Les Renardières (FR)
- an intermodel comparison between our code developed in Matlab environment and TRNSYS

Concerning the validation at the BESTLab, the results show that the model is able to predict the temperature evolution of the internal air and the envelope's internal surfaces with good accuracy, with residuals lying always within a range of ± 1 °C. The residuals of the walls' internal surface temperature are higher on days characterized by clear sky conditions (and thus high beam radiation). The discrepancies could be attributed to an imperfect knowledge of the window's thermo-optical properties and/or to the modelling of the impinging solar radiation (e.g. shading effect due to the West wall). More in general, other possible sources of discrepancy between measurements and predictions could be related to (i) an imperfect knowledge of the envelope's material properties and the thermal bridges, (ii) measurement issues (no re-calibration of some sensors) and (ii) internal errors in the form of model simplifications (e.g. hygrothermal phenomena are not modelled).

The intermodel comparison is conducted in two phases. The first phase can be considered a *model verification* (Section 1.1): the outputs of specific algorithms used in the *Matlab code* to calculate astronomical variables and the sky-dome temperature have been checked against TRNSYS, which provided the benchmark. The second phase of the intermodel comparison checks the level of agreement between the *Matlab code* and TRNSYS as concerns the global thermal behaviour of a virtual test cell. The correspondence between the two software tools is generally good, with residuals of the internal air temperature and the mean radiant temperature lying most of the time within a range of ± 0.5 °C. The residuals are significantly lower for the intermodel comparison, partly because input values are in this case not affected by uncertainty. The lumped-parameter approach, although requiring a longer computation time compared to the transfer-function approach, provides information on the temperature evolution of the various layers of the envelope, which becomes important to determine the variation of internal energy of the envelope, as done in [19] for the calorimetric heat balance of a test cell. This validation work was performed in order to increase the confidence in both the model and the optimised design of calorimetric experiments proposed in [19].

## Acknowledgements

We gratefully knowledge the contribution of Thierry Duforestel, Mathilde Colmet Daâge and Hervé Castet from EDF R&D who provided the experimental data and precious support to the experimental validation activity. The present work has been partially developed within the framework of EU Cost Action TU1403 "Adaptive Facades Network".

## References

[1] T. Trucano, L. Swiler, T. Igusa, W. Oberkampf, M. Pilch, Calibration, validation: and sensitivity analysis: what's what, Reliab. Eng. Syst. Saf. 91 (2006) 1331–1357.
[2] E. Palomo del Barrio, G. Guyon, Application of parameters space analysis tools for empirical model validation, Energy Build. 36 (2004) 23–33.
[3] S. Moinard, G. Guyon, Empirical Validation of EDF ETNA and GENEC Test-cell Models, A Report of Task 22, Subtask A.3 Empirical Validation, International Energy Agency, 1999.
[4] T. Mara, F. Garde, H. Boyer, M. Mamode, Empirical validation of the thermal model of a passive solar cell test, Energy Build. 33 (2001) 589–599.
[5] F. Miranville, H. Boyer, T. Mara, F. Garde, On the thermal behaviour of roof-mounted radiant barriers under tropical and humid climatic conditions: modelling and empirical validation, Energy Build. 35 (2003) 997–1008.
[6] E. Allen, D. Bloomfield, N. Bowman, K. Lomas, J. Allen, J. Whittle, A. Irving, Analytical and Empirical Validation of Dynamic Thermal Building Models. Proceedings of BS1985, 274–280, Seattle, USA, 1985.
[7] R. Judkoff, D. Wortman, B. O'Doherty, J. Burch, A Methodology for Validating Building Energy Analysis Simulations, National Renewable Energy Laboratory, Golden, CO, 2008.
[8] R. Judkoff, D. Wortman, J. Burch, Measured Versus Predicted Performance of the SERI Test House: A Validation Study Golden, Solar Energy Research Institute, Colorado, 1983.

[9] H. Eppel, K. Lomas, Empirical Validation of Three Thermal Simulation Programs Using Data from a Passive Solar Building. Proceedings of Building Simulation 1995, Adelaide, Australia, 1995, pp. 588–595.
[10] R. Judkoff, D. Wortman, J. Burch, Empirical Validation of Building Analysis Simulation Programs: A Status Report, Solar Energy Research Institute, Colorado, 1982.
[11] ANSI/ASHRAE, Standard 140–2007-Standard Method of Test for the Evaluation of Building Energy Analysis Computer Programs, 2007 (Atlanta).
[12] D. Xiao, Inter-model, Analytical, and Experimental Validation of a Heat Balance Based Residential Cooling Load Calculation Procedure, Faculty of the Graduate College of the Oklahoma State University, Oklahoma, USA, 2006.
[13] J. Neymark, P. Girault, G. Guyon, R. Judkoff, R. LeBerre, J. Ojalvo, P. Reimer, The ETNA BESTEST empirical validation data set, in: Proceedings of BS2005, Montréal, Canada, 2005, pp. 839–846.
[14] R. Judkoff, J. Neymark, The BESTEST Method for Evaluating and Diagnosing Building Energy Sloftware Proceedings of Energy Efficiency in a Competitive Environment, USA, 1998, pp. 5.175–5.192.
[15] S. Jensen, Validation of building energy simulation programs: a methodology, Energy Build. 22 (1995) 133–144.
[16] A. Irving, Validation of dynamic thermal models, Energy Build. 10 (1988) 213–220.
[17] P. Strachan, G. Kokogiannakis, I. Macdonald, History and development of validation with the ESP-r simulation program, Build. Environ. 43 (2008) 601–609.
[18] G. Cattarin, F. Causone, A. Kindinis, L. Pagliano, Outdoor test cells for building envelope experimental characterization –a literature review, Renew. Sustain. Energy Rev. 54 (2016) 606–625.
[19] L. Pagliano, G. Cattarin, F. Causone, A. Kindinis, Calorimetric determination of the solar factor in outdoor test cell facilities, Energy Build. 153 (2017) 513–524.
[20] E. Ryan, T. Sanquist, Validation of building energy modeling tools under idealized and realistic conditions, Energy Build. 47 (2012) 375–382.
[21] IBPSA-USA, IBPSA-USA. (n.d.). BEST Directory, 2017, Retrieved from http://www.buildingenergysoftwaretools.com/.
[22] EDF, Description De La Cellule RDC Ouest Du Laboratoire BESTLab., 2016.
[23] NF EN 13829. Performance Thermique Des bâtiments – Détermination De La Perméabilité à l'air Des bâtiments – Méthode De Pressurisation Par Ventilateur, 2001.
[24] LBL, WINDOW 4.1, PC program for analyzing window thermal performance in accordance with standard NFRC procedures, in: Windows and Daylighting Group, Building Technologies Program, Energy and Environment Division, Lawrence Berkeley Laboratory, 1994.
[25] G. Cattarin, PhD Dissertation. On the Calorimetric Measurement of the Solar Factor of Transparent Building Components in Outdoor Test Cell Facilities, Politecnico di Milano, Milan, 2017.
[26] A. Rodler, Modélisation Dynamique Tridimensionnelle Avec Tache Solaire Pour La Simulation Du Comportement Thermique d'un bâtiment Basse Consommation (in French), INSA de Lyon, 2014.
[27] G. Fraisse, C. Viardot, O. Lafabrie, G. Achard, Development of a simplified and accurate building model based on electrical analogy, Energy Build. 34 (2002) 1017–1031.
[28] M. Gouda, S. Danaher, C. Underwood, Building thermal model reduction using nonlinear constrained optimization, Build. Environ. 37 (2002) 1255–1265.
[29] A. Khalifa, R. Marshall, Validation of heat transfer coefficients on interior building surfaces using a real-sized indoor test cell, Int. J. Heat Mass Transf. 33 (1990) 2219–2236.
[30] A. Hatton, H. Awbi, Convective Heat Transfer in Rooms. Building Simulation '95, Fourth International Conference Proceedings, Madison, USA, 1995, pp. 221–227.
[31] W. Rohsenow, J. Hartnett, Y. Cho, Handbook of Heat Transfer, 3rd ed., McGraw-Hill, 1998.
[32] K. Chatziangelidis, D. Bouris, Calculation of the distribution of incoming solar radiation in enclosures, Appl. Therm. Eng. 29 (2009) 1096–1105.
[33] K. Kontoleon, Dynamic thermal circuit modelling with distribution of internal solar radiation on varying façade orientations, Energy Build. 47 (2012) 139–150.
[34] ASHRAE, Fundamental Handbook, ASHRAE, 2009.
[35] J. Duffie, W. Beckman, Solar Engineering of Thermal Processes, John Wiley & Sons Inc, New York, 1991.
[36] M.G. Davies, Building Heat Transfer, Wiley, 2004.
[37] Berkely Lab, Lab. WINDOW v7.4.8.0, 2016.
[38] G. Guyon, S. Moinard, N. Ramdani, Validation of the CLIM2000 Software Program by Using Analytical Verification Proceedings of Building Simulation'99 (1999).
[39] NFRC, NFRC 201–210 – Procedure for Interim Standard Test Method for Measuring the Solar Heat Gain Coefficient of Fenestration Systems Using Calorimetry Hot Box Methods Greenbelt, National Fenestration Rating Council, USA, 2010.
[40] S. Bontemps, Validation Expérimentale De Modèles: Application Aux bâtiments Basse Consommation (in French), Université de Bordeaux, 2015.
[41] M. Martin, P. Berdahl, Characteristics of infrared sky radiation in the United States, Sol. Energy 33 (3/4) (1984) 321–336.